ANALYTICAL ELECTROMECHANICAL MODEL FOR CMUTS WITH MULTI-LAYERED, NON-UNIFORM-THICKNESS DIAPHRAGM

P. Pursula[1,2], J. Saarilahti[1], O. Paul[2], and V. Viikari[1]

[1] *VTT Technical Research Centre of Finland, Espoo, Finland*
[2] *IMTEK Department of Microsystems Engineering, University of Freiburg, Freiburg, Germany*

***Abstract* — In this paper we present for the first time an analytical electromechanical model for capacitive micromachined ultrasonic transducers (CMUTs) with multi-layered diaphragms of non-uniform thickness. The model is based on dynamical Kirchhoff plate theory, which allows to derive the accurate static deflection and vibration mode, and hence the mechanical and electrical impedance of the transducer. Experimental verification of the model is provided by measurements of electrical impedance and transmission in air. Resonant frequencies given by the model deviate less than 2 % from the measured results.**

Keywords: **CMUT, analytical model, non-uniform diaphragm**

I – Introduction

Capacitive micromachined ultrasonic transducers (CMUTs) have been studied widely in recent years. These small and reliable ultrasonic transducers promise novel applications in medical ultrasonic imaging and implantable systems, such as intravascular imaging [1].

Even though the on modelling CMUTs have been addressed in many papers, e.g. [4], there is a need for analytical treatment of nonuniform resonant diaphragms. Fabrication techniques often favor nonuniform diaphragms and nonuniformity can also be used to adjust the transmission properties of a CMUT. In this paper we present a model for such multi-layered plates as well as plates with nonuniform thickness.

The schematic of the hexagonal transducer is presented in Fig. 1 [2]. Lower electrode is made of poly-Silicon, and the air cavity has a pressure of about 1 mBar. The diaphragm has three layers (Tables 1 and 2), of which SiN is an insulator, and the top-electrode is consists of poly-Si together with Aluminium. The poly-Si and Al are deposited only on a central part of the diaphragm. Hence the diphragm thickness is a function of the radial coordinate, and it can be divided to radial sections with differing constant plate thicknesses. The model presented can be used for any number of layers and any number of radial sections.

II – Model

A. Vibration Mode

The hexagonal geometry of the CMUT device is modelled with a circular diaphragm of the same area,

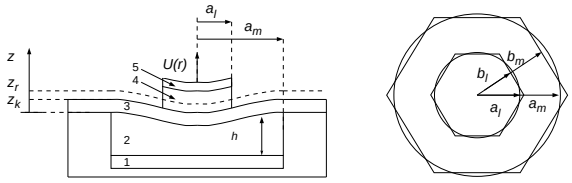

Figure 1: *Device schematic. The dashed line represents the reference plane. Layer numbering refers to Table 2.*

giving $a^2 = (2\sqrt{3}/\pi)b^2$ for all radial measures. The analytical model is based on dynamical Kirchhoff plate theory (e.g. [3]), which gives for circular plates the equation of motion

$$D\nabla^4 U(r,t) - \tau\nabla^2 U(r,t) + p - R\frac{\partial U(r,t)}{\partial t} = \rho_s \frac{\partial^2 U(r,t)}{\partial t^2}, \quad (1)$$

where $U(r,t)$ is the deflection, D the flexural stiffness, τ the tensile stress per unit length, and ρ_s the surface density of the diaphragm; R describes the viscous losses and external pressure p is the sum of the electrical p_e and athmospheric pressures p_a acting on the diaphragm.

First, we assume small vibrations $u(r,t)$ around a static deflection $u_0(r)$, i.e. $U(r,t) = u_0(r) + u(r,t)$. We define an effective gap h_{eff} of the capacitor by averaging the static deflection over the diaphragm, and taking into account the insulating SiN layer, i.e.

$$h_{eff} = h_{air} + h_{SiN}\frac{\varepsilon_{air}}{\varepsilon_{SiN}} + \frac{1}{\pi a^2}\int_0^a 2\pi r u_0(r). \quad (2)$$

where h_{air} is the undeflected air gap thickness. Now the electrical pressure can be written as a Taylor series

$$p_e = -\frac{\varepsilon_0 V_{dc}^2}{2h_{eff}^2} - \frac{\varepsilon_0 V_{dc} V_{ac}(t)}{h_{eff}^2} + \frac{\varepsilon_0 V_{dc}^2 u(r,t)}{h_{eff}^3}. \quad (3)$$

For sinusoidal excitations $V_{ac}(t) = V_{ac}e^{j\omega t}$ and vibrations $u(r,t) = u(r)e^{j\omega t}$, Eq. 1 can be arranged to two separate equations, one for static displacement u_0 and one for the complex vibration amplitude u

$$\begin{aligned} \nabla^2\left(D\nabla^2 - \tau_0\right)u_0(r) &= p_a + \frac{\varepsilon_0 V_{dc}^2}{2h_{eff}^2}, \\ D\left(\nabla^2 + \frac{\alpha^2}{a^2}\right)\left(\nabla^2 - \frac{\beta^2}{a^2}\right)u(r) &= \frac{\varepsilon_0 V_{dc}}{h_{eff}^2}V_{ac}, \end{aligned} \quad (4)$$

Table 1: *Material parameters.*

Material	ρ (kg/m^3)	σ (MPa)	E (GPa)	ν	ε_r
SiN	3440	248	165	0.25	7.5
poly-Si	2330	160	160	0.22	11.7
Al	2700	70	70	0.35	–

Table 2: *Device structure.*

Layer	Material	h (nm)	a_{in} (μm)	a_{out} (μm)
5	Al	1000	15.5	18
4	poly-Si	380	0	18
3	SiN	420	0	22
2	Air	300	0	22
1	poly-Si	—	0	22

where

$$\begin{aligned}
\alpha^2 &= \varphi\left(\sqrt{1+\frac{(Ka)^4}{\varphi^2}}-1\right),\\
\beta^2 &= \varphi\left(\sqrt{1+\frac{(Ka)^4}{\varphi^2}}+1\right),\\
K^4 &= \frac{\omega^2\rho_s}{D}+\frac{\varepsilon V_{dc}^2}{Dd_0^3}-j\omega\frac{R}{D},\\
\varphi &= \frac{\tau a^2}{2D},\\
D &= \frac{Eh^3}{12(1-\nu^2)}.
\end{aligned} \tag{5}$$

Here a is the radius, E Young's modulus, h the thickness, ν the Poisson's ratio, and line stress $\tau=\sigma h$, where σ is the stress. Both Equations in 4 are expressed as a product of two second order differential operators. The solution of the equations is the sum of the general solutions of the homogenous differential equations defined by the individual operators, plus a particular solution of the full inhomogenious equation [5]. We proceed to solve the Equation for static deflection u_0 first.

The general solution in cylinderical coordinates is

$$\begin{aligned}
u_0(r) &= A_0+B_0\ln(r)-\frac{r^2}{4\tau}\left(p_a+\frac{\varepsilon_0 V_{dc}^2}{2h_{air}^2}\right)\\
&+ C_{0,n}I_n(\beta r/a)+F_{0,n}K_n(\beta r/a),
\end{aligned} \tag{6}$$

where I_n and K_n are the nth-order modified Bessel functions of the first and second kind, and A_0, B_0, $C_{0,n}$ and $F_{0,n}$ are constants to be determined from the boundary conditions. The relevant solution here is formed by the zeroth order Bessel functions. We use gap h_{air} for static solution u_0, which gives the effictive gap h_{eff} by averaging over the diaphragm area (see Eq. 2).

The stiffening of the spring, i.e. the deformation induced increase in the tensile line stress τ is calculated as [6]

$$\tau=\tau_0+\frac{D_0}{2a}\int_0^a\left(\frac{\partial u_0(r)}{\partial r}\right)^2 dr, \tag{7}$$

where $D_0=E/(1-\nu^2)$ is the stretching stiffness of the plate.

Now the general solution for the complex vibration amplitude can be written as

$$\begin{aligned}
u(r) &= A_nJ_n(\alpha r/a)+B_nY_n(\alpha r/a)\\
&+ C_nI_n(\beta r/a)+F_nK_n(\beta r/a)\\
&+ \frac{\varepsilon_0 V_{dc}V_{ac}}{h_{eff}^2 DK^4},
\end{aligned} \tag{8}$$

where J_n and Y_n are the Bessel functions of the first and second kind, and A_n, B_n, C_n and F_n are constants to be determined from the boundary conditions. We are interested in the lowest operation mode, and hence it is adequate to consider the lowest order $n=0$ of the Bessel functions. The average displacement $\hat{u}=1/(\pi a^2)\int_0^a 2\pi r u(r)dr$ is used for calculating the mechanical impedance Z_m of the diaphragm, which is defined by the ratio of force $f=p_e\pi a^2$ acting on the diaphragm and the average velocity $\hat{v}=j\omega\hat{u}$ of the diaphragm , i.e. [4]

$$Z_m=\frac{p_E\pi a^2}{j\omega\hat{u}}. \tag{9}$$

The derived general solution allows us to calculate the deflection $u(r)$ for different geometries, also for nonuniform plates. Vibrations in uniform diaphragms are treated e.g. in [4], to which our solution reduces at the limit of vanishing cavity pressure. Hence we concentrate on the nonuniform case.

B. Non-uniform Diaphragms

We consider two kinds of nonuniformities: multilayered diaphragms, where the materials and mechanical parameters change as a function of vertical coordinate z, and concentric changes in diaphragm thickness, leading to separate radial sections with uniform thickness.

Multilayered structures can be treated as single layered structures by calculating effective mechanical parameters of the structure [6]. For this we define a reference plane that behaves as the "neutral plane" in bending of multilayered diaphragms. The position of the reference plane within the stack is calculated as

$$z_r=\frac{\sum_{k=1}^n E_k(z_k^2-z_{k-1}^2)}{2\sum_{k=1}^n E_k(z_k-z_{k-1})}, \tag{10}$$

where z_k is the vertical coordinate of the upper surface of the kth layer (see Fig. 1). Now, for n stacked layers, the effective density per unit area $\hat{\rho}_s$, line force $\hat{\tau}$ and streching stiffness $\hat{D}_0$ are calculated as sums over the layers

$$\begin{aligned}
\hat{\rho}_s &= \sum_{k=1}^n \rho_k(z_k-z_{k-1})\\
\hat{\tau} &= \sum_{k=1}^n \sigma_k(z_k-z_{k-1})\\
\hat{D}_0 &= \sum_{k=1}^n \frac{E_k}{1-\nu_k^2}(z_k-z_{k-1}),
\end{aligned} \tag{11}$$

where ρ_k is the density, σ_k the tensile stress, and E_k the Young's modulus in the kth layer. Now the effective flexural stiffness can be calculated as

$$\hat{D}=\sum_{k=1}^n \frac{E_k}{3(1-\nu_k^2)}\left[(z_k-z_r)^3-(z_{k-1}-z_r)^3\right]. \tag{12}$$

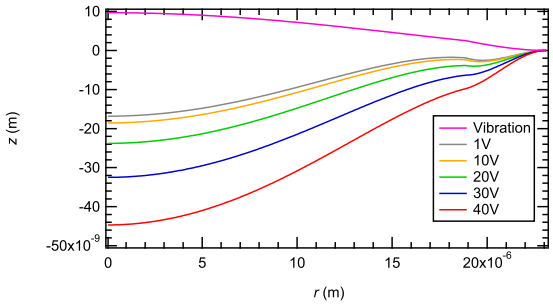

Figure 2: *Static displacement of the diaphragm with various bias voltages, and dynamic deflection mode at resonance (V_{dc} = 40 V, f = 4.16 MHz).*

Further, the multilayer may impose an initial bending moment S_0, which appears in the boundary conditions

$$S_0 = \sum_{k=1}^{n} \frac{\sigma_k}{2} \left[(z_k - z_r)^2 - (z_{k-1} - z_r)^2 \right]. \qquad (13)$$

With these definitions, the multilayered diaphragm can be treated as single layered one by replacing the mechanical parameters by the effective ones.

To analyse concentric changes in diaphragm thickness, we divide diaphragm in m radial sections of uniform thickness, solve Eq. 4 in every section l to obtain solutions $U_l(r)$. Then we apply boundary conditions of the form for $0 < l < m$

$$\begin{aligned}
&U_m(a_m) = 0,\ U'_m(a_m) = 0,\\
&U_{l+1}(a_l) = U_l(a_l),\\
&\hat{D}_{0,l+1} U'_{l+1}(a_l) + \tau_{l+1} = \hat{D}_{0,l} U'_l(a_l) + \tau_l,\\
&-\hat{D}_{l+1}\left(U''_{l+1}(a_l) + \frac{\nu_{l+1}}{a_l} U'_{l+1}(a_l) \right) + S_{0,l+1}\\
&= -\hat{D}_l \left(U''_l(a_l) + \frac{\nu_l}{a_l} U'_l(a_l) \right) + S_{0,l}\\
&\hat{D}_{l+1}\left(U'''_{l+1}(a_l) + \frac{1}{a_l} U''_{l+1}(a_l) + \frac{1}{a_l^2} U'_{l+1}(a_l) \right) + \frac{p_{l+1} a_l}{2}\\
&= \hat{D}_l \left(U'''_l(a_l) + \frac{1}{a_l} U''_l(a_l) + \frac{1}{a_l^2} U'_l(a_l) \right) + \frac{p_l a_l}{2}\\
&U_0(0) = \text{ finite}, \qquad (14)
\end{aligned}$$

where a_l is the outer radius of the lth section of the diaphragm. The boundary conditions between the sections at $a_0 \ldots a_{m-1}$ describe the continuity of deflection, in-plane force, bending moment and vertical force, respectively.

The analytical solution consists of a lengthy sum of Bessel functions and therefore it is not presented here. Instead, we illustrate the results in graphical form. We modelled the device in two radial sections: Outer section with SiN, and an inner section with flexural properties given by Si and SiN. Aluminium was considered only as a mass loading in the inner section. The static deformations produced by the model can be seen in Fig. 2. The bend at $r \approx 18$ μm is due to the initial bending moment S_0 of the inner section.

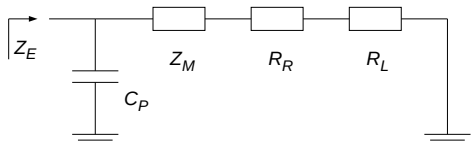

Figure 3: *The Electomechanical model for the CMUT array.*

C. Losses

The viscous damping by air is explicitly introduced into the mechanical model. Because no squeeze film damping occurs, we use Stokes drag force approximation, i.e. $R_v = 6\gamma_{air}/a_m$.

For a circular piston the radiation resistance is approximately given by $R_r = \rho_{air} c_{air} \pi a_m^2$ [7], if the area of the piston is larger than the wavelength. This is not strictly true for a single CMUT diaphragm, but if the whole array is considered, the approximation is valid. We model the radiation losses as a mechanical resistance R_r external to the mechanical model.

All other loss mechnanism are bundled together in an external resistance R_l. This includes anchor losses, losses introduced by nonidealities, as well as electrical series losses in the array.

D. Electromechanical Model

The mechanical impedance of a N-cell CMUT array can be constructed by adding the acoustic impedances of the single elements.The mechanical and electrical impedances are linked by the transduction factor $k = C_0 V_{dc}/h_{eff}$, and the static capacitance of the CMUT elements $C_P = NC_0$ is added in parallel (see Fig. 3). In our device, N = 346, and the electrical impedance is

$$Z_E = \left(j\omega C_P + \frac{Nk^2}{Z_m + R_r + R_l} \right)^{-1}. \qquad (15)$$

III – Experimental results

The CMUT arrays were bonded on a LTCC carrier, and their electrical impedance was measured with HP4294A impedance analyzator, which was calibrated to the carrier pins. The measured and modelled electrical impedances at V_{dc} = 40 V are shown in Fig. 4. The measured and modelled results are highly similar, when one takes into account that the model does not include any fitted paramaters. Loss modelling is still inadequate, which was to be expected, because here R_l = 0. Also a constant shift in the vertical direction is observed, which can be explained by additional parallal capacitance due to e.g. non-modelled chip-carrier and in-chip paracitic capacitance. Adding parallel capacitance of 5.7 pF and mechanical loss $R_l = 2R_r$, the model approaches the measured results. From this we get an approximate radiation efficiency of 30 %. In Fig. 5 the measurement and modelled impadences, with added paracitic capacitance and loss terms, are compared at several bias voltages. The resonant frequency is modelled within 2% at all bias levels.

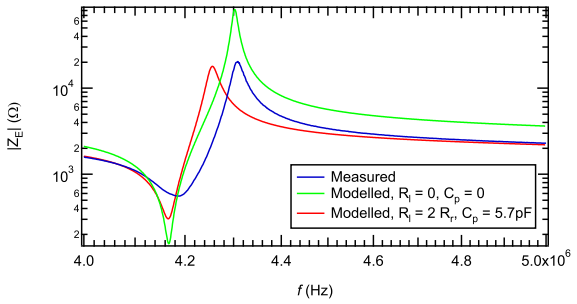

Figure 4: *Electrical impedance of the CMUT at V_{dc} = 40 V.*

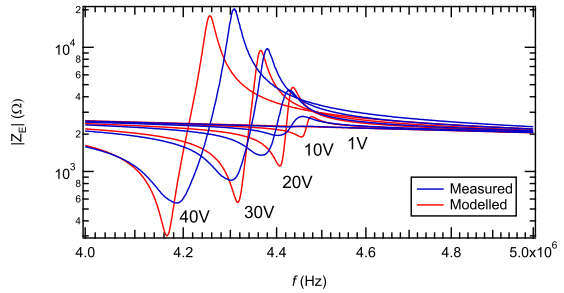

Figure 5: *Electrical impedance of the CMUT with different bias voltages.*

To further characterize the CMUT devices and to validate the mechanical model, a transmission measurement between two CMUTs was carried out. Two devices were placed coaxially facing each other, and transmission between the devices was measured. For this purpose, a PCB board with driver and LNA amplifiers was designed.

The signal propagation between CMUTs was modelled with the Frii's free space equation including a 1000-dB/m air attenuation [7]. CMUTs transmission and reception gain G is relative to the gain of a losless and isotropic ultrasonic radiator. The measured and simulated transmission curves for a distance of 5 mm can be seen in Fig. 6. The undulation of the signal is due to standing waves between the transmitter and receiver. The simulated curve is fitted to the measured one using CMUT impeance and G as variable parameters. The fit resulted in G = 40–120, depending on the devices and transmission distance.

The theoretical directivity of a piston radiator is approximately $(ka)^2$, and the array factor towards the main beam is N [7]. Hence the efficiency η of the CMUT, i.e. the ratio of radiation losses and all losses can be calculated as $\eta = G/N(ka)^2 \approx 3$–$10$ %. This is somewhat lower than given by the model. However, the far-field criterion was not fulfilled in the transmission measurement, and any deviation in the excitation phase of the CMUTs over the array diminishes the directivity. Further measurements are required to define the radiation efficiency with greater accuracy.

In many applications, e.g. in medicine, the devices will be used in liguids or tissue, ehere the radiation resistance will be manyfold, because the acoustic impedance ρc will increase tremendously, e.g. over

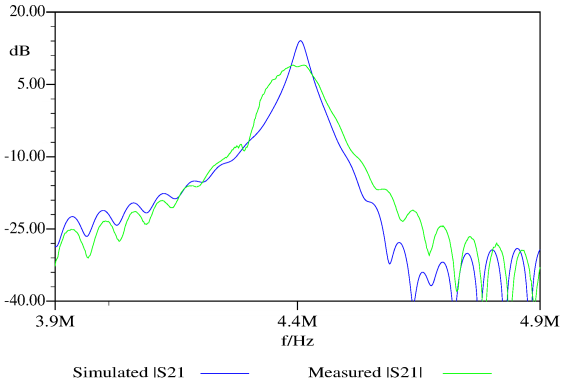

Figure 6: *Transmission between CMUTs at a distance of 5.2 mm including amplifier gain. The fit gives G= 120.*

thousand-fold for water. The other loss mechanisms do not scale with the acoustic impedance, and high efficiency is expected. Future work includes model development and measurement of the device in water.

IV – Conclusion

This paper described for the first time a electromechanical model for CMUTs with nonuniform and multilayered diaphragms based on dynamical Kirchhoff plate theory. Using only the geometrical dimensions and material parameters, the measured and modelled resonant frequencies differed less than 2 %. Radiation losses were included in the model, and an external resistance was added to account for other loss mechanisms. Transmission efficiency of the CMUT was estimated to be around 5-30 % in air. Radiation in water is expected to be much higher, whereas other loss mechanisms do not increase as much. Hence higher radiation efficiency is expected in water.

References

[1] D. T. Yeh, Ö. Oralkan, I. O. Wygant, M O'Donnell, and B. T. Khuri-Yakub, *IEEE Trans. on Ultrasonics, Ferroelectrics, and Frequency Control*, 53:1202–1211, 2006.

[2] J. Saarilahti, M. Blomberg, A. Häärä, H. Kattelus, *IEEE Ultrasonics Symposium*, pp. 1071–1074, 2002.

[3] O. A. Bauchau, J. I. Craig, *Structural Analysis*, Springer Netherlands, 2009.

[4] A. Caronti, G. Caliano, A. Iula, M. Pappalardo, *IEEE Trans. on Ultrasonics, Ferroelectrics and Frequency Control*, 49:159–168, 2002.

[5] T. Wah, *Journal of the Acoustical Society of America*, 34:275–281, 1962.

[6] O. Paul, J. Gaspar, *Advanced Micro and Nanosystems*, 6:67–121, 2008.

[7] L. E. Kinsler, A. R. Frey, A- B. Coppens, J. V. Sanders, *Fundamentals of Acoustics*, John Wiley & Sons, 2000.